

# Near Threshold Effects on Recombination and Vibrational Relaxation in Efimov Systems

D. Shu, I. Simbotin, R. Côté

*Department of Physics, University of Connecticut, Storrs, CT 06268, USA*

We investigate the energy dependence of inelastic processes in systems which possess Efimov states. We consider the three-body recombination rate  $K_3$  where three free atoms interact to produce an atom-dimer pair, and the relaxation rate  $K_{\text{rel}}$  where an atom quenches a weakly bound state of a dimer near an Efimov resonance to more deeply bound levels. Using a model capturing the key features of the Efimov problem, we identify new energy regimes for  $K_3$ , namely the NTR (Near Threshold Resonance) regime behavior  $E^{-2}$  for negative scattering lengths and the NTS (Near Threshold Suppression) regime behavior  $E^2$  for positive scattering lengths. We also confirm a previously found oscillatory behavior of  $K_3$  at higher energy  $E$ . Finally, we find that  $K_{\text{rel}}$  behaves as  $E^{-1}$  in the NTR regime.

## I. INTRODUCTION

Three-body problems have been studied in a variety of context, such as three-body Coulomb systems [1–3], and nuclear three-body systems [4–6]. Efimov predicted that a system with three particles may have a large number of trimer states even when the dimer potential does not possess any bound states [7–9]. The existence of the Efimov trimer states requires the two-body scattering length  $a$  to be much larger than the characteristic range of the two-body interaction  $R_0$ . Ultracold gases are ideal candidates for studying Efimov physics since the scattering length  $a$  can be tuned using Feshbach resonances. When  $a \rightarrow -\infty$ , an Efimov state near the three-body threshold will give a resonant enhancement for the recombination rate  $K_3$ . This enhancement has been experimentally observed as atom loss for a variety of systems [10–24]. When  $a \rightarrow +\infty$ , a similar enhancement has been observed for the vibrational relaxation rate  $K_{\text{rel}}$  for collisions between atoms and loosely bound dimers [18, 19, 21, 25, 26]. Resonant peaks for atom loss rates have also been observed for pure ultracold atom gases with  $a > 0$  [12, 27, 28], and an avalanche mechanism has been proposed as an explanation in terms of molecule-atom threshold resonances [12, 27], though other experiments have been conducted pointing to different conclusion [29, 30]. For  $a \rightarrow +\infty$ , interference minima as a signature of Efimov states in three atom loss rates have also been observed [12, 13, 27, 28, 31].

Efimov physics has been studied mostly in the zero energy limit, e.g., the recombination and relaxation rates near zero temperature, and only recently the energy dependence of these quantities has received attention [32–37]. In this paper, we investigate the energy dependence of the three body recombination rate  $K_3$  and relaxation rate  $K_{\text{rel}}$ , paying special attention to the threshold behavior of  $K_3(E)$  for  $a < 0$  and  $K_{\text{rel}}(E)$  for  $a > 0$  when an Efimov state is near the threshold. We also explore the behavior of  $K_3(E)$  for  $a > 0$  for specific values of  $a$  leading to large suppression effects.

## II. THE MODEL

In this work, we study the Efimov effect for the case of identical bosons, BBB, where B denotes a neutral bosonic atom in its ground state. Our findings are however also ap-

plicable to other systems (such as mixtures of the type BBX) which have a similar attractive Efimov potential. In addition, we only consider the case of total angular momentum  $J = 0$ , which is sufficient at low energy where contributions of higher  $J$  values are strongly suppressed.

Although the long range Efimov states seem counterintuitive, their appearance can be explained by the attractive  $1/R^2$  behavior of the lowest adiabatic hyperspherical potential for  $R_0 \ll R \ll |a|$ , where  $R$  is the hyperradius, and  $a$  and  $R_0$  are the two-body scattering length and characteristic interaction range, respectively. The attractive Efimov potential takes the form [38]

$$V_{\text{Ef}}(R) = -\frac{s_0^2 + 1/4}{R^2}, \quad (1)$$

where  $s_0 = 1.00624$  is a universal constant. Following [38], the appropriate reduced mass is implicitly included in  $V_{\text{Ef}}(R)$ ; the same is true throughout the article for all potentials. According to Efimov [7], when  $a \rightarrow \pm\infty$ , the number of three-body Efimov states is proportional to  $\ln(|a|/R_0)$ , and is independent of the sign of  $a$ . However, the lowest adiabatic hyperspherical potential depends on the sign of  $a$ . Specifically, when  $a < 0$ , the Efimov potential correlates in the asymptotic region  $R \gg |a|$  to the repulsive potential

$$V_{\text{asy}}(R) = \frac{\ell_{\text{eff}}(\ell_{\text{eff}} + 1)}{R^2}, \quad (2)$$

with  $\ell_{\text{eff}} = \frac{3}{2}$ , which is the lowest three-body continuum channel. Again,  $V_{\text{asy}}$  contains the reduced mass. In this case, the three-body recombination rate  $K_3$  exhibits a resonant enhancement when an Efimov state is near the three-body breakup threshold. When  $a > 0$ , the effect of the Efimov states on the three-body loss rates is quite different, which is due to the fact that the Efimov potential correlates to the weakly bound dimer channel. Following Esry et al. [38], we employ a simplified model which captures the essential physics of the Efimov effect.

### A. Single-channel model for $a < 0$

For  $a < 0$ , the entrance channel is the lowest three-body continuum channel, and all other channels corresponding to

the three-body continuum can be ignored since their hyperspherical adiabatic potentials are entirely repulsive; their contribution will be highly suppressed at low energy. We assume that the dimer has deeply bound states, which is typical for atom-atom potentials, and we shall use a single channel model to analyze the three-body recombination. The recombination channels corresponding to the deeply bound dimer states are taken into account *a posteriori*, as explained in this section. The fact that the coupling of the entrance channel to the recombination channels takes place at short range ( $R < R_0$ ) allows for a single-channel model of the multi-channel problem that reproduces qualitatively the energy dependence of  $K_3$  [32]. To extract  $K_3(E)$  from the single-channel results, we use an approach based on the Jost function, as opposed to the wave function as used by [32]. Namely, we obtain the single-channel regular solution  $\phi_k(R)$  by numerically solving

$$\phi_k''(R) = [V_1(R) - k^2]\phi_k(R), \quad (3)$$

where  $V_1$  is the potential curve shown in Fig. 1. Note that for  $R_0 \ll R \ll |a|$ ,  $V_1(R) \approx V_{\text{Ef}}(R)$  and for  $R \gg |a|$ ,  $V_1(R) \approx V_{\text{asy}}(R)$ . Equation (3) is supplemented with the initial condition  $\phi_k(R_0) = \sin \varphi_0$  and  $\phi_k'(R_0) = \cos \varphi_0$ , where the phase  $\varphi_0$  accounts for the contribution of the short range region. As shown in the inset in Fig. 1, the parameter  $\varphi_0$  can be adjusted to obtain agreement with the experimental results for the value of  $a_1^-$  of the two-body scattering length corresponding the appearance of first Efimov state. However, in the remainder of our paper, we employ the simple choice  $\varphi_0 = 0$  which corresponds to a hard wall at  $R = R_0 = R_{\text{vdW}}$ . The two-body van der Waals length  $R_{\text{vdW}}$  is the characteristic length scale for the short range region, with  $R_{\text{vdW}} = (2\mu_2 C_6/\hbar^2)^{1/4}$ , where  $\mu_2$  is the two-body reduced mass and  $C_6$  the dispersion coefficient for the van der Waals interaction ( $-C_6/R^6$ ) between two neutral ground state atoms.  $R_{\text{vdW}}$  and the corresponding van der Waals energy  $E_{\text{vdW}} = \hbar^2/2\mu_2 R_{\text{vdW}}^2$  are used as units in Fig. 1.

We extract the Jost function

$$F(k) = A(k) - iB(k) \quad (4)$$

from the asymptotic ( $R \rightarrow \infty$ ) behavior  $k^{\ell_{\text{eff}}+1}\phi_k(R) \sim A(k)j_{\ell_{\text{eff}}}(kR) + B(k)n_{\ell_{\text{eff}}}(kR)$ , where  $j_{\ell_{\text{eff}}}$  and  $n_{\ell_{\text{eff}}}$  are the Riccati-Bessel spherical functions. Note that  $V(R)$  and  $k$  are real, and thus  $\phi_k$ ,  $A(k)$  and  $B(k)$  are also real. The physical solution  $\psi_k$ , which behaves asymptotically as  $\psi_k(R) \sim \frac{i}{2}[h_{\ell_{\text{eff}}}^-(kR) - \frac{F^*}{F}h_{\ell_{\text{eff}}}^+(kR)]$ , where  $h_{\ell}^{\pm} \equiv n_{\ell} \pm ij_{\ell}$ , can be expressed as [39]

$$\psi_k = \frac{k^{\ell_{\text{eff}}+1}}{F(k)}\phi_k. \quad (5)$$

For very low  $k$ , the regular solution is independent of  $k$  at short range,  $\phi_k(R) \approx \phi_0(R)$ . Thus, at short range, we have

$$\psi_k(R)|_{\text{short range}} \approx \frac{k^{\ell_{\text{eff}}+1}}{F(k)}\phi_0(R), \quad (6)$$

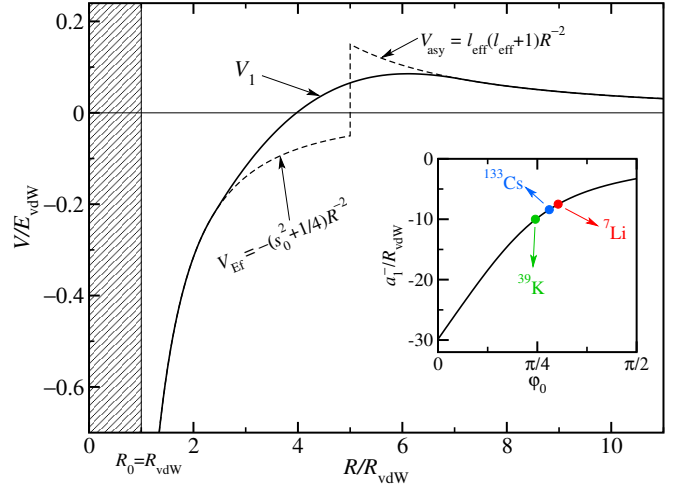


FIG. 1: Lowest hyperspherical potential for  $a = -5R_{\text{vdW}}$ . Solid line: smooth approximation for the realistic hyperspherical potential  $V_1(R)$  in Eq. (3). The shaded area represents the short range region  $0 < R < R_0$ , taken into account via the phase  $\varphi_0$  appearing as a parameter for the initial condition at  $R_0 = R_{\text{vdW}}$  for Eq. (3). Dotted line: approximate potential (discontinuous at  $R = |a|$ ) used in Sec. III A. The inset shows the  $\varphi_0$  dependence of the scattering length  $a_1^-$  corresponding to the appearance of the first Efimov state. Also shown are three experimental results for Cs, K and Li [38] illustrating how  $\varphi_0$  can be adjusted to match experiments.

Returning to the multi-channel problem, and noting that the coupling of the entrance channel to the deeply bound states of the dimer takes place at short range, the entrance channel component  $\psi_{1,k}$  of the full wave function can be approximated by the single-channel solution (5), i.e.,

$$\psi_{1,k} \approx \psi_k = \frac{k^{\ell_{\text{eff}}+1}}{F(k)}\phi_k \quad (7)$$

Since the couplings are restricted to short range, the single channel result in Eq. (6) can be used to obtain the  $k$  dependence of the full solution of the coupled-channel problem [40]. Indeed, the  $k$ -dependence in Eq. (6) will be imprinted via the couplings to all other components of the wave function. We emphasize that, although the entrance-channel component has the  $k$ -dependence in Eq. (6) only at short range, the other components obey this  $k$ -dependence for all  $R$ ,

$$\psi_{n,k} \sim \frac{k^{\ell_{\text{eff}}+1}}{F(k)}g_n(k_n, R), \quad (8)$$

where  $g_n(k_n, R)$  is the radial wave function for channel  $n$  with momentum  $k_n$ . Recalling that only outgoing waves are allowed in the dimer channels  $n$ , the corresponding asymptotic ( $R \rightarrow \infty$ ) behavior of  $\psi_{n,k}$  is

$$\psi_{n,k}(R) \sim \sqrt{\frac{k}{k_n}}S_{n,1}(k)e^{+ik_n R}. \quad (9)$$

Together with Eq. (8) and substituting  $2\ell_{\text{eff}} + 1 = 4$ , it leads to the  $k$ -dependence of the S-matrix element,

$$|S_{n,1}(k)|^2 \sim \frac{k^4}{|F(k)|^2}. \quad (10)$$

Finally, the total three-body recombination rate [41],  $K_3 \sim \frac{1}{k^4} \sum_{n \neq 1} |S_{n,1}|^2$ , reads

$$K_3 \sim \frac{1}{|F(k)|^2} = \frac{1}{A^2(k) + B^2(k)}. \quad (11)$$

Thus, the  $k$ -dependence of the rate  $K_3$  is dictated by the  $k$ -dependence of the Jost function.

### B. Single-channel model for relaxation ( $a > 0$ )

As shown in Fig. 2 for the case  $a > 0$ , there exists a loosely bound dimer state (channel 2, slightly below the three-body breakup threshold) which correlates to the Efimov potential, while the lowest three-body continuum channel is purely repulsive (channel 1). In channel 2, the three-body system corresponds to an extended weakly bound Feshbach molecule interacting with an atom. Since decay into more deeply bound and compact dimers takes place due to short-range couplings, a single-channel model similar to the case  $a < 0$  described in Sec. II A above is warranted for the rate of the vibrational relaxation rate  $K_{\text{rel}}$ , which will thus be expressed in terms of the single channel Jost function.

In this case, we have an atom-dimer scattering problem with relative angular momentum  $\ell$ , so that one simply replaces  $\ell_{\text{eff}}$  by  $\ell$  in Eqs. (7) and (8), leading to

$$|S_{fi}(k)|^2 \sim \frac{k^{2\ell+1}}{|F(k)|^2}. \quad (12)$$

We are interested in  $\ell = 0$  (ultracold regime), so that the cross section  $\sigma = \frac{\pi}{k^2} \sum_{f \neq i} |S_{fi}(k)|^2$  for this inelastic process gives the relaxation rate  $K_{\text{rel}} = v_{\text{rel}} \sigma$  (with the relative velocity  $v_{\text{rel}} \propto k$ ) in terms of the S-matrix as [41]

$$K_{\text{rel}}(k) \sim \frac{1}{k} \sum_{f \neq i} |S_{fi}|^2, \quad (13)$$

Here,  $i$  and  $f$  correspond to the entrance (shallow) dimer state, and final (deeply bound) dimer states respectively. The S-matrix is given in term of the Jost function by Eq. (12) with  $\ell = 0$ , i.e.,

$$|S_{fi}(k)|^2 \sim \frac{k}{|F(k)|^2}. \quad (14)$$

Combining the two equations above, we find the  $k$ -dependence of the relaxation rate,

$$K_{\text{rel}}(k) \sim \frac{1}{|F(k)|^2} = \frac{1}{A^2(k) + B^2(k)}. \quad (15)$$

### C. Two-channel model for $a > 0$

As discussed above for  $a > 0$ , and as illustrated in Fig. 2, there exists a loosely bound dimer state (channel 2) correlated

to the Efimov potential, while the lowest three-body continuum channel being purely repulsive (channel 1). Therefore, to investigate the three-body recombination for the formation of Feshbach molecules, we adopt a model that only includes these two channels:

$$\begin{aligned} \phi_1'' &= [V_{11} - k_1^2] \phi_1 + [V_c \partial_R + \partial_R V_c] \phi_2 \\ \phi_2'' &= [V_{22} - k_2^2] \phi_2 - [V_c \partial_R + \partial_R V_c] \phi_1. \end{aligned} \quad (16)$$

According to [38], the coupling between channel 1 and channel 2 is significant only near  $R = a$ . Thus we employ a simple form for the coupling,

$$V_c(R) = \begin{cases} \frac{0.01}{a} \sin^4\left(\pi \frac{R-R_a}{R_b-R_a}\right), & R_a < R < R_b \\ 0, & \text{otherwise} \end{cases} \quad (17)$$

with  $R_a = 0.5a$ ,  $R_b = 1.5a$ . Note that the scaling  $V_c(R) \sim a^{-1}$  follows the realistic coupling, and the value 0.01 for the coefficient controlling the strength of the coupling in Eq. (17), chosen arbitrarily, can be adjusted to match experimental data for a particular system [38]. In the region  $R_0 \ll R \ll a$  we have

$$V_{11}(R) \approx \frac{s_1^2 - 1/4}{R^2}, \quad V_{22}(R) \approx V_{\text{Ef}} = -\frac{s_0^2 + 1/4}{R^2}, \quad (18)$$

where  $s_1 = 4.4653$  and  $V_{\text{Ef}}$  is the Efimov potential in Eq. (1). In the asymptotic region  $R \gg |a|$ ,

$$V_{11}(R) \approx \frac{\ell_{\text{eff}}(\ell_{\text{eff}} + 1)}{R^2}, \quad V_{22}(R) \approx E_b, \quad (19)$$

where  $E_b \propto -1/a^2$  is the binding energy of the shallow dimer. In the region near  $R = a$ ,  $V_{11}(R)$  and  $V_{22}(R)$  are connected smoothly between the inner and outer regions using high order polynomials; namely, we ensure their continuity and the continuity of their first and second derivatives.

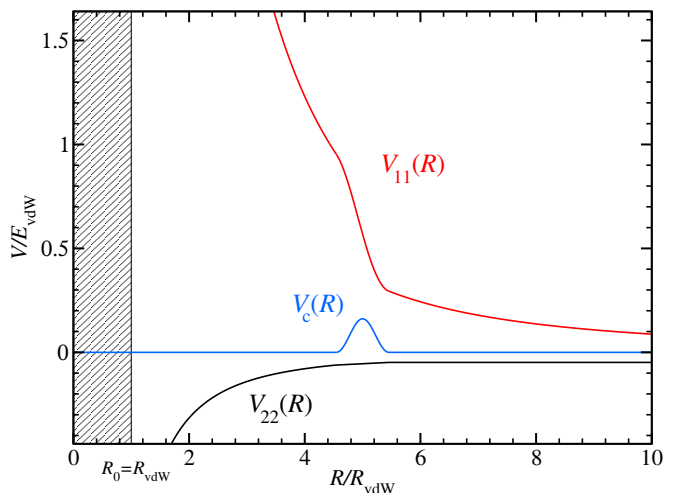


FIG. 2: Schematic representation of the potentials used in the two channel model, see Eqs. (16,17). Red curve: hyperspherical potential for channel 1. Black curve: hyperspherical potential for channel 2 corresponding to the shallow dimer state. Blue curve: coupling potential  $V_c$  which is non-zero only near  $R = a$ . The shaded area represents the short range region.

### III. RESULTS

In this section, we discuss the  $k$ -dependence of rate coefficients for the various cases introduced in the previous sections.

#### A. Single channel results for $a < 0$

Using the model described in Sec. II A, we carefully tune the two-body scattering length  $a$  such that there is an Efimov state extremely close to the threshold. Here, since there is only one channel corresponding to the three free atoms, the threshold refers to it (see Fig. 1). In Fig. 3, we show results for the first five Efimov states. Although arbitrary units are used for the three-body recombination rate  $K_3$  in Fig. 3, one could introduce a multiplicative parameter on the right hand side of Eqs. (10) and (11) to adjust the overall magnitude of  $K_3$  to match experimental values. In Fig. 3(a), the black curve corresponds to  $a_1^-/R_{\text{vdW}} = -29.865651$  and displays the first Efimov state as a shape resonance located at very low energy, while the red and blue curves correspond to  $a = 2a_1^-$  and  $a = a_1^-/2$  respectively. We found that the resonant behavior manifests itself only for values of  $a$  within one percent of  $a_1^-$ . For values of  $a$  outside of this narrow window, the behavior is similar to that shown by the red and blue curves, which we call non-resonant. Although the sharp peak at very low energy is striking, this near threshold resonance (NTR) produces a resonant enhancement for a much wider energy range. More specifically, Fig. 3(a) shows that in the resonant case most of the low energy regime is characterized by a new type of behavior; namely,  $k^4 K_3$  is constant for energies between the peak and vertical dashed line at  $E = E_1$ , which we refer to as the NTR regime. For the subsequent Efimov states corresponding to  $a_n^-$  with  $n = 2, 3, 4, 5$ , an oscillatory regime develops [32] in the energy range  $E_n < E < E_0$  between the two vertical dashed lines, as shown in Fig. 3(b)–(e).  $E_0 = E_{\text{vdW}}$  denotes the energy scale associated with short-range physics, while  $E_n \equiv E_{a_n^-}$  with  $E_a = (R_{\text{vdW}}/a)^2 E_{\text{vdW}}$  the energy scale given by the centrifugal barrier near  $R = |a|$  in Fig. 1. With increasing  $|a|$ , a new Efimov state will appear for each critical value  $a_n^-$ , and we confirm the well known result  $a_{n+1}^-/a_n^- = e^{\pi/s_0}$ . Our results also confirm that as  $|a|$  increases, more oscillations appear at lower energies (reflecting the number of bound states), while the oscillations at higher energy remain unchanged [32], as shown in Fig. 3, and summarized in Fig. 4.

Although the results in Figs. 3 and 4 were obtained using the smooth potential shown in Fig. 1, the oscillatory behavior can be explained by writing the wavefunction corresponding to the step potential in Fig. 1 in terms of Bessel functions. For  $R_0 < R < |a|$  the regular solution defined in Sec. II A can be written as linear combination of Bessel functions of imaginary order,

$$\begin{aligned} \tilde{j}(kR) &\equiv \sqrt{\frac{\pi kR}{2}} \operatorname{sech}\left(\frac{\pi s_0}{2}\right) \operatorname{Re}[J_{is_0}(kR)] \\ \tilde{n}(kR) &\equiv \sqrt{\frac{\pi kR}{2}} \operatorname{sech}\left(\frac{\pi s_0}{2}\right) \operatorname{Re}[Y_{is_0}(kR)]. \end{aligned} \quad (20)$$

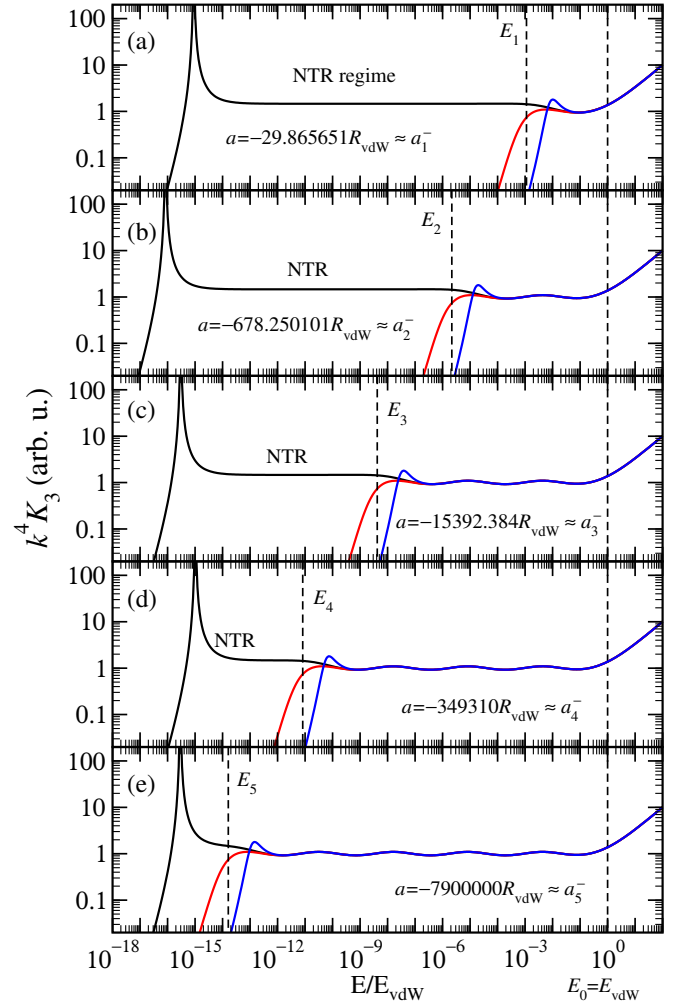


FIG. 3: Three-body recombination rates for  $a < 0$ . Black curves: resonant cases for the first five Efimov states (the values of  $a \approx a_n^-$  are indicated). Red and blue curves: non-resonant cases corresponding to  $a = 2a_n^-$  and  $a = a_n^-/2$  respectively. The dashed vertical line at  $E_0 = E_{\text{vdW}}$  marks the energy scale associated with short range physics. The dashed vertical lines at  $E_n \equiv E_{a_n^-} \propto 1/(a_n^-)^2$  mark the boundary between the NTR and oscillatory regimes.

Using the small argument behavior [42] near  $R \approx R_0$ ,

$$\begin{aligned} \tilde{j}(kR) &\sim \left(\frac{t_0 kR}{s_0}\right)^{\frac{1}{2}} \cos[s_0 \ln\left(\frac{kR}{2}\right) - \gamma_{s_0}] \\ \tilde{n}(kR) &\sim \left(\frac{kR}{t_0 s_0}\right)^{\frac{1}{2}} \sin[s_0 \ln\left(\frac{kR}{2}\right) - \gamma_{s_0}], \end{aligned} \quad (21)$$

where  $\gamma_{s_0} = \arg[\Gamma(1 + is_0)]$  and  $t_0 = \tanh(\frac{\pi s_0}{2})$ . Thus the suitable linear combination for the regular solution is

$$\begin{aligned} \phi_k(R) &= \left(\frac{R_0 t_0}{s_0 k}\right)^{\frac{1}{2}} \left( \cos[s_0 \ln\left(\frac{kR_0}{2}\right) - \gamma_{s_0}] \tilde{j}(kR) \right. \\ &\quad \left. - t_0^{-1} \sin[s_0 \ln\left(\frac{kR_0}{2}\right) - \gamma_{s_0}] \tilde{n}(kR) \right). \end{aligned} \quad (22)$$

For  $R > |a|$ , as mentioned in Sec. II A, the regular solution can be written as a linear combination of the Riccati-Bessel

functions

$$k^{\ell_{\text{eff}}+1} \phi_k(R) = A(k) j_{\ell_{\text{eff}}}(kR) + B(k) n_{\ell_{\text{eff}}}(kR). \quad (23)$$

By matching at  $R = |a|$ , i.e., equating the expressions in Eq. (22) and Eq. (23) and their derivatives, and using the behavior at large argument [42] near  $R = |a|$ ,

$$\begin{aligned} \tilde{j}(kR) &\sim \cos(kR - \frac{\pi}{4}) \\ \tilde{n}(kR) &\sim \sin(kR - \frac{\pi}{4}) \end{aligned} \quad (24)$$

we obtain

$$\begin{aligned} A(k) &= k^2 \left( \frac{R_0}{s_0 t_0} \right)^{\frac{1}{2}} \sin[s_0 \ln(\frac{kR_0}{2}) - \gamma_{s_0}] \\ B(k) &= k^2 \left( \frac{R_0 t_0}{s_0} \right)^{\frac{1}{2}} \cos[s_0 \ln(\frac{kR_0}{2}) - \gamma_{s_0}], \end{aligned} \quad (25)$$

where  $\gamma_{s_0} = \arg[\Gamma(1 + i s_0)]$  and  $t_0 = \tanh(\frac{\pi s_0}{2})$ . Therefore, inside the oscillatory regime, the three-body recombination rate reads,

$$K_3(k) \sim \frac{1}{k^4} \frac{s_0 t_0}{R_0} \frac{1}{t_0 + (1 - t_0) \sin^2[s_0 \ln(\frac{kR_0}{2}) - \gamma_{s_0}]}. \quad (26)$$

Note that the amplitude of the oscillatory term,  $1 - t_0 \approx 0.081$ , is much smaller than the background term  $t_0 \approx 0.92$ , which makes it difficult to discern the difference between the NTR regime and the oscillatory regime in Fig. 3. For  $k \ll |a|^{-1}$ , the Jost function can be expanded as a power series,  $A(k) \sim A_0 + A_2 k^2 + \mathcal{O}(k^4)$  and  $B(k) \sim k^{2\ell_{\text{eff}}+1} (B_0 + B_2 k^2 + \dots) = B_0 k^4 + \mathcal{O}(k^6)$  (since  $\ell_{\text{eff}} = 3/2$ ) [40]. Using Eq. (11), we obtained a simple expression of the three-body recombination rate,

$$K_3(k) \sim \frac{1}{(A_0 + A_2 k^2)^2 + B_0^2 k^8}. \quad (27)$$

In the Wigner regime,  $A_0$  is dominant, and the zero energy limit of  $K_3$  is a constant. For the resonant case  $A_0$  is very small, which restricts the Wigner regime to the extreme ultracold. Thus when  $k$  increases, the  $A_2 k^2$  term quickly becomes dominant and  $K_3(k)$  reads,

$$K_3(E) \sim \frac{1}{k^4 A_2^2}, \quad (28)$$

which corresponds to the flat NTR regime shown in Fig. 4 for  $k^4 K_3$ . Note that the transition between Wigner and NTR regimes takes place near  $k_{\text{NTR}} = \sqrt{|A_0/A_2|}$ , which can be estimated from the simple parametrizations  $A_0(a) \propto a - a_n^-$  and  $A_2(a) \approx A_2(a_n^-) = \text{const.}$  in the narrow window of values of  $a$  near  $a_n^-$ . Fig. 4(a) and Fig. 3 show the Efimov states as shape resonances, which correspond to the case when  $A_0$  and  $A_2$  have opposite sign, such that  $A(k) = 0$  at  $k_{\text{NTR}}$ . Note that the very small but finite term  $B_0^2 k^8$  in Eq. (27) will prevent  $K_3$  from diverging. In Fig. 4(b), the Efimov states are bound just below the three-body threshold, which corresponds to the case when  $A_0$  and  $A_2$  have the same sign. Thus  $B_0^2 k^8$  can be neglected in Eq. (27), and the transition between the Wigner and NTR regimes is smooth. We emphasize that the  $K_3 \sim k^{-4}$  behavior in the NTR regime is accidentally identical to the background  $k$ -dependence in the oscillatory regime in Eq. (26), though the exact values are offset as depicted in Fig. 4.

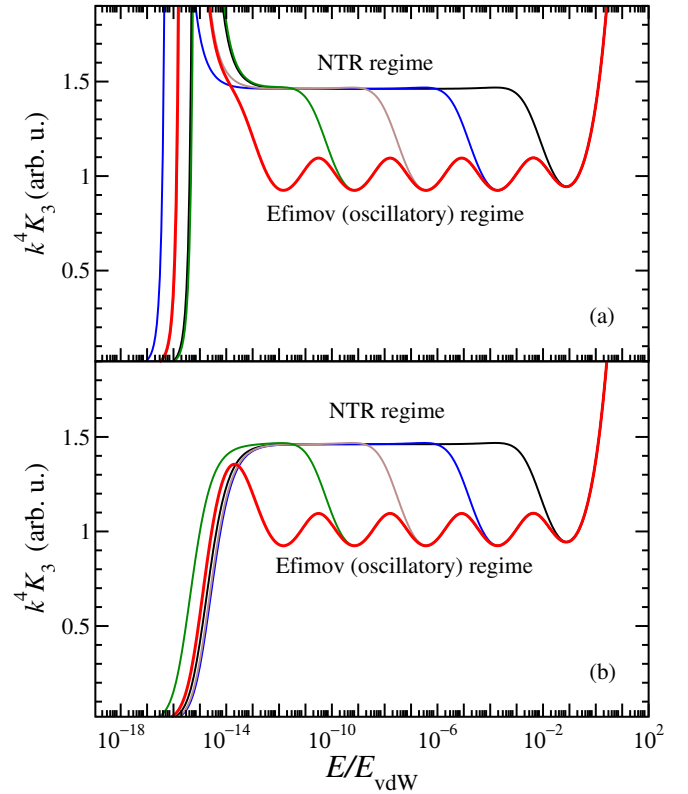


FIG. 4: (a)  $K_3$  for the case when the Efimov states are shape resonances just above the threshold; these are the black curves from Fig. 3. (b)  $K_3$  for the case when the Efimov states are bound just below the threshold corresponding to values of  $|a|$  slightly larger than the values in Fig. 3.

## B. Single channel results for $a > 0$

When  $a > 0$ , the Efimov potential correlates with the weakly bound dimer channel, defining the scattering threshold  $k = 0$ . We expect that a near threshold Efimov state will strongly affect the Feshbach-molecule–atom collisions, resulting in vibrational relaxation into deeply bound dimer states. Here we analyze the vibrational relaxation rate using the single-channel model described in Section II B, with the vibrational relaxation rate given by Eq. (15),

$$K_{\text{rel}}(k) \sim \frac{1}{|F(k)|^2}. \quad (29)$$

Note that  $F(k)$  is the single channel Jost function corresponding to the lower potential curve in Fig. 2.

For energies higher than the binding energy of the shallow dimer state,  $E_b \sim -1/a^2$ , but lower than the short range energy scale  $E_0 \sim 1/R_0^2$ , i.e.,  $a^{-1} \ll k \ll R_0^{-1}$ , using Eq. (22) again, but this time matching it with the asymptotic form of  $\phi_k(R)$  for  $\ell = 0$ , namely

$$k \phi_k(R) = A(k) \sin(kR) + B(k) \cos(kR), \quad (30)$$

we obtain

$$\begin{aligned}
A(k) &= \sqrt{k} \left( \frac{R_0 t_0}{2s_0} \right)^{\frac{1}{2}} \left( \cos[s_0 \ln(\frac{kR_0}{2}) - \gamma_{s_0}] \right. \\
&\quad \left. - \frac{1}{t_0} \sin[s_0 \ln(\frac{kR_0}{2}) - \gamma_{s_0}] \right) \\
B(k) &= -\sqrt{k} \left( \frac{R_0 t_0}{2s_0} \right)^{\frac{1}{2}} \left( \cos[s_0 \ln(\frac{kR_0}{2}) - \gamma_{s_0}] \right. \\
&\quad \left. + \frac{1}{t_0} \sin[s_0 \ln(\frac{kR_0}{2}) - \gamma_{s_0}] \right),
\end{aligned} \tag{31}$$

and thus,  $K_{\text{rel}}(k)$  reads,

$$K_{\text{rel}} \sim \frac{1}{k} \frac{s_0 t_0}{R_0} \frac{1}{t_0^2 + (1 - t_0^2) \sin^2[s_0 \ln(\frac{kR_0}{2}) - \gamma_{s_0}]}. \tag{32}$$

The overall  $k^{-1}$  behavior of the relaxation rate in Eq. (32) was already mentioned in Ref. [32], where however no oscillatory behavior was found. In our case, we do obtain an oscillatory behavior for  $K_{\text{rel}}(k)$  similar to that of  $K_3(k)$ . As shown in Fig. 5, this oscillatory behavior resembles the oscillations in Fig. 3. The dashed curves in Fig. 5 correspond to non-resonant cases, while the solid curves show the resonant cases for the first three Efimov states near the threshold.

For  $k \ll a^{-1}$ ,  $A(k)$  and  $B(k)$  can be written as a power series:  $A(k) \sim A_0 + A_2 k^2 + \mathcal{O}(k^4)$  and  $B(k) = k^{2\ell+1}(B_0 + B_2 k^2 + \dots) \sim B_0 k + \mathcal{O}(k^3)$  (with  $\ell = 0$ ). As a result the relaxation rate reads

$$K_{\text{rel}}(k) \sim \frac{1}{(A_0 + A_2 k^2)^2 + B_0^2 k^2}. \tag{33}$$

$A_0$  is very small for the resonant case and thus the competition between  $A_0$  and  $B_0^2 k^2$  gives the Wigner and NTR regimes. In the Wigner regime,  $A_0$  is dominant and  $K_{\text{rel}}$  is a constant when  $k$  goes to zero, while in the NTR regime  $K_{\text{rel}} \sim 1/B_0^2 k^2$  since  $B_0^2 k^2$  becomes dominant in the denominator of Eq. (33) as we increase  $k$ . In contrast to Eq. (27), the  $A_2 k^2$  term no longer plays a significant role and we omit it from Eq. (33); indeed,  $A_2^2 k^4$  is a higher order term which can be neglected, while the cross term  $2A_0 A_2 k^2$  can be combined with  $B_0^2 k^2$  which is equivalent to altering  $B_0$  very slightly. Hence we obtain

$$K_{\text{rel}}(k) \sim \frac{1}{A_0^2 + B_0^2 k^2}. \tag{34}$$

This equation captures the transition between the Wigner and NTR regimes. The transition is smooth whether or not the Efimov state is just above or below the threshold.

### C. Two channel results for $a > 0$

When the atom-atom scattering length  $a$  is positive and large, there is a shallow dimer state just below the threshold, and we use the 2-channel model introduced in Sec. II C to compute the three-body recombination rate for the process  $B + B + B \rightarrow B + B_2$  (shallow). As is well known [9], the zero energy limit of the three-body recombination rate  $K_3$

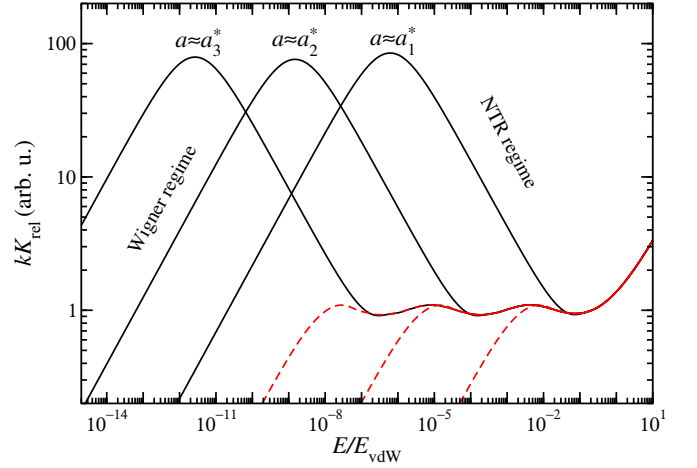


FIG. 5: Black curves: vibrational relaxation rate for three values of  $a = a_n^*$  as indicated, corresponding to the first, second and third Efimov state near the threshold, with  $a_1^* = 11.45 R_{\text{vdW}}$ ,  $a_2^* = 260.0 R_{\text{vdW}}$ , and  $a_3^* = 5902.0 R_{\text{vdW}}$ , respectively. Red curves: relaxation rate for the non-resonant cases with  $a = 3a_n^*$  for each curve, respectively.

is a log-periodic function of the dimer scattering length  $a$ , as shown in Fig. 6a. Each maximum in Fig. 6a corresponds to an Efimov state at the dimer-atom threshold [9], which does not affect the energy dependence of  $K_3$ . However, each minimum in Fig. 6a corresponds to a critical value of  $a$  for which the energy dependence of  $K_3$  is dramatically modified as shown in Fig. 6b. The dashed line in Fig. 6b corresponds to a non-critical case, when  $K_3(k)$  follows Wigner's threshold law for  $k \ll a^{-1}$ . The other three curves in Fig. 6b correspond to the three minima in Fig. 6a, for which the three-body recombination rate displays a strongly suppressed behavior  $K_3(k) \sim k^4$  for  $k_{\text{NTS}} \ll k \ll a^{-1}$ , that we label the *Near Threshold Suppression* (or NTS) regime.

The numerical solution for the 2-channel model is obtained as follows. The regular matrix solution  $\Phi$  is initialized at  $R = R_0$  using boundary conditions corresponding to a hard wall,  $\Phi(R_0) = 0$  and  $\Phi'(R_0) = \mathbf{I}$ , where  $\mathbf{I}$  is the  $2 \times 2$  unit matrix. After propagation, and recalling that  $\ell = \ell_{\text{eff}}$  for channel 1, and  $\ell = 0$  for channel 2, the regular solution is matched to asymptotic solutions,

$$\Phi \mathbf{k}^{\ell+1} = \mathbf{f} \mathbf{A} + \mathbf{g} \mathbf{B}, \tag{35}$$

where  $\mathbf{k}^{\ell+1} = \text{diag}(k_1^{\ell_{\text{eff}}+1}, k_2)$  and  $\mathbf{f}$  and  $\mathbf{g}$  are diagonal matrices containing the single channel asymptotic solutions  $f_1 = j_{\ell_{\text{eff}}}(k_1 R)$ ,  $g_1 = n_{\ell_{\text{eff}}}(k_1 R)$ ,  $f_2 = \sin(k_2 R)$  and  $g_2 = \cos(k_2 R)$ . The matrices  $\mathbf{A}$  and  $\mathbf{B}$  are the real and imaginary parts of the Jost matrix  $\mathbf{F} = \mathbf{A} - i\mathbf{B}$ . The expression of the S-matrix in terms of the Jost matrix reads

$$S_{21} = \sqrt{\frac{k_2}{k_1}} (\mathbf{F}^* \mathbf{F}^{-1})_{21} = 2i \sqrt{\frac{k_2}{k_1}} \frac{A_{22} B_{21} - A_{21} B_{22}}{\det(\mathbf{F})}. \tag{36}$$

Using the power series of the Jost matrix elements when  $k \ll$

$a^{-1}$ , we obtain

$$S_{21}(k_1) = k_1^2 \frac{C_0 + C_2 k_1^2}{D_0 + D_2 k_1^2}. \quad (37)$$

Recalling Eq. (11), we find

$$K_3 \sim \frac{1}{k_1^4} |S_{21}|^2 = \left| \frac{C_0 + C_2 k_1^2}{D_0 + D_2 k_1^2} \right|^2. \quad (38)$$

For the values of  $a$  corresponding to the strongly suppressed NTS cases shown in Fig. 6b, the Efimov states are not near the threshold. This implies that the S-matrix does not exhibit a resonant structure, i.e., it has no nearby pole, or equivalently,  $\det(\mathbf{F}) \neq 0$  or simply  $D_0 \neq 0$  in the limit  $k_1 \rightarrow 0$ . Hence the low  $k_1$  behavior of the three-body recombination rate  $K_3$  is determined by the competition between  $C_0$  and  $C_2 k_1^2$  in Eq. (38). In the Wigner regime,  $C_0$  is dominant and thus  $K_3$  is nearly constant. Note that normally, the Wigner regime behavior is valid for  $k_1 \ll a^{-1}$ , while in the NTS case  $C_0$  is vanishingly small and the Wigner regime is restricted to  $k_1 \ll k_{\text{NTS}} = \sqrt{|C_0/C_2|}$ . As Fig. 6b clearly shows, there is a new type of behavior for  $k_{\text{NTS}} \ll k_1 \ll a^{-1}$ , where  $C_2 k_1^2$  in Eq. (37) is dominant, and thus  $K_3 \sim k_1^4$ .

#### IV. CONCLUSION

In this paper, we studied the effect of Efimov states on the energy dependence of three-body recombination rates  $K_3(E)$  and vibrational relaxation rates  $K_{\text{rel}}(E)$  for shallow dimers. We used simple models capturing the essential physical processes. For negative atom-atom scattering length,  $a < 0$ , a single-channel model is used to express  $K_3$  in term of a single-channel Jost function. For positive scattering length,  $a > 0$ , we use a single-channel model expressing the vibrational relaxation  $K_{\text{rel}}$  in term of a single-channel Jost function, while a two-channel model is used to obtain  $K_3$ . We used the analytical structure and properties of Jost functions to explain the numerical results obtained by varying the scattering energy  $E$  (or momentum  $k$ ) for given values of  $a$ .

When the atom-atom scattering length  $a$  is negative, we recovered the usual Wigner regime at ultralow energies, but as  $a$  gets very close to an Efimov resonance, we uncovered a new regime, labeled Near Threshold Resonance (or NTR) regime where  $k^4 K_3 \sim \text{const.}$  (or low energy behavior  $K_3(E) \sim E^{-2}$ ). We also recover the oscillatory behavior obtained in other studies. Similarly, when  $a \rightarrow +\infty$ , we find the relaxation rate to reach a constant at ultralow energy, corresponding to the Wigner regime, and if an Efimov state is at the threshold,  $K_{\text{rel}} \sim k^{-2} \propto E^{-1}$ , corresponding again to the NTR regime. In addition, we found oscillations about a  $k^{-1}$  behavior for  $k$  corresponding to energies larger than the NTR regime.

Finally, for  $a \rightarrow +\infty$ , we found that the usual Wigner behavior  $K_3 \sim \text{const.}$  for the rate of three-body recombination (into a shallow dimer) is strongly suppressed near the threshold. It behaves as  $k^4$  or  $K_3(E) \sim E^2$  when the atom-atom

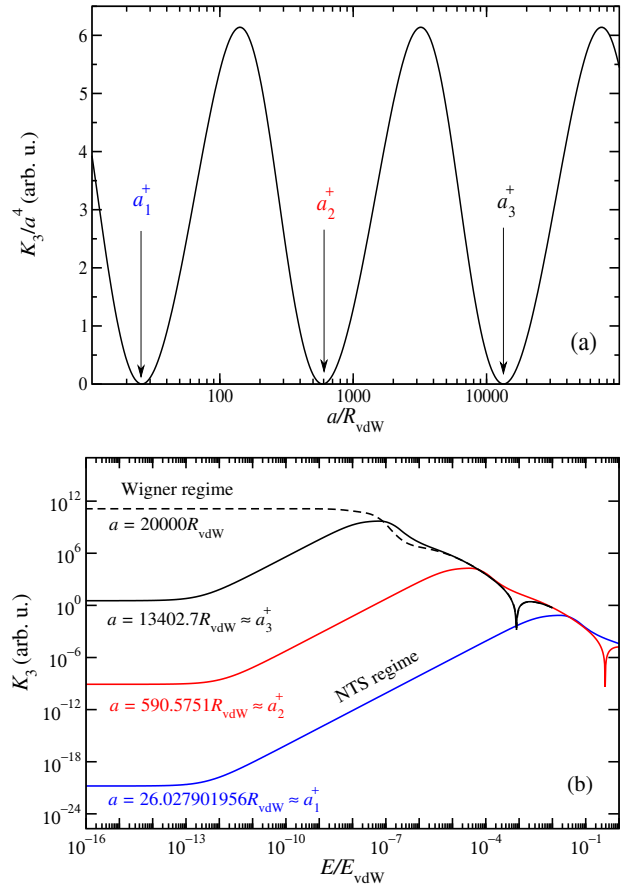


FIG. 6: (a)  $K_3$  in the limit  $E \rightarrow 0$  as function of  $a$ . The positions  $a_n^+$  of the minima are indicated and their values are given in the lower panel. (b) Dashed line:  $K_3(E)$  for non-critical case, which displays only the Wigner regime behavior at low energy. Solid lines: first three critical cases corresponding to the minima in the upper panel. The minima of  $K_3(E)$  appearing at energies between  $E/E_{\text{vdW}} = 10^{-4}$  and  $E/E_{\text{vdW}} = 1$  are due to destructive interference as explained in Ref. [33].

scattering length nears one of the critical values corresponding to the minima of  $K_3$  as a function of  $a$  (in the zero energy limit). This new regime, labeled the Near Threshold Suppression regime (NTS), could potentially be used to stabilize cold gases by preventing three-body recombination by adjusting the two-body scattering length to one of the large and positive critical values of  $a$ .

#### V. ACKNOWLEDGMENT

The authors wish to thank Dr. Jia Wang for fruitful discussions. This work was partially supported by the US Army Research Office, Chemistry Division, Grant No. W911NF-13-1-0213 (DS), and by the MURI US Army Research Office Grant No. W911NF-14-1-0378 (IS and RC).

- [1] J. P. Neirrotti, P. Serra, and S. Kais, *Phys. Rev. Lett.* **79**, 3142 (1997), URL <http://link.aps.org/doi/10.1103/PhysRevLett.79.3142>.
- [2] P. Serra, J. P. Neirrotti, and S. Kais, *Phys. Rev. Lett.* **80**, 5293 (1998), URL <http://link.aps.org/doi/10.1103/PhysRevLett.80.5293>.
- [3] S. Kais and Q. Shi, *Phys. Rev. A* **62**, 060502 (2000), URL <http://link.aps.org/doi/10.1103/PhysRevA.62.060502>.
- [4] V. Efimov, *Phys. Rev. C* **44**, 2303 (1991), URL <http://link.aps.org/doi/10.1103/PhysRevC.44.2303>.
- [5] V. Efimov, *Phys. Rev. C* **47**, 1876 (1993), URL <http://link.aps.org/doi/10.1103/PhysRevC.47.1876>.
- [6] E. Garrido, D. V. Fedorov, and A. S. Jensen, *Phys. Rev. Lett.* **96**, 112501 (2006), URL <http://link.aps.org/doi/10.1103/PhysRevLett.96.112501>.
- [7] V. Efimov, *Soviet Journal of Nuclear Physics* **12** (1971).
- [8] V. Efimov, *Physics Letters B* **33**, 563 (1970), ISSN 0370-2693, URL <http://www.sciencedirect.com/science/article/pii/0370269370903497>.
- [9] E. Braaten and H.-W. Hammer, *Physics Reports* **428**, 259 (2006), ISSN 0370-1573, URL <http://www.sciencedirect.com/science/article/pii/S0370157306000822>.
- [10] T. Kraemer, M. Mark, P. Waldburger, J. G. Danzl, C. Chin, B. Engeser, A. D. Lange, K. Pilch, A. Jaakkola, H.-C. Nägerl, et al., *Nature* **440**, 315 (2006).
- [11] J. R. Williams, E. L. Hazlett, J. H. Huckans, R. W. Stites, Y. Zhang, and K. M. O'Hara, *Phys. Rev. Lett.* **103**, 130404 (2009), URL <http://link.aps.org/doi/10.1103/PhysRevLett.103.130404>.
- [12] S. E. Pollack, D. Dries, and R. G. Hulet, *Science* **326**, 1683 (2009).
- [13] N. Gross, Z. Shotan, S. Kokkelmans, and L. Khaykovich, *Phys. Rev. Lett.* **105**, 103203 (2010), URL <http://link.aps.org/doi/10.1103/PhysRevLett.105.103203>.
- [14] M. Berninger, A. Zenesini, B. Huang, W. Harm, H.-C. Nägerl, F. Ferlaino, R. Grimm, P. S. Julienne, and J. M. Hutson, *Phys. Rev. Lett.* **107**, 120401 (2011), URL <http://link.aps.org/doi/10.1103/PhysRevLett.107.120401>.
- [15] R. J. Wild, P. Makotyn, J. M. Pino, E. A. Cornell, and D. S. Jin, *Phys. Rev. Lett.* **108**, 145305 (2012), URL <http://link.aps.org/doi/10.1103/PhysRevLett.108.145305>.
- [16] S. Roy, M. Landini, A. Trenkwalder, G. Semeghini, G. Spagnolli, A. Simoni, M. Fattori, M. Inguscio, and G. Modugno, *Phys. Rev. Lett.* **111**, 053202 (2013), URL <http://link.aps.org/doi/10.1103/PhysRevLett.111.053202>.
- [17] T. B. Ottenstein, T. Lompe, M. Kohnen, A. N. Wenz, and S. Jochim, *Phys. Rev. Lett.* **101**, 203202 (2008), URL <http://link.aps.org/doi/10.1103/PhysRevLett.101.203202>.
- [18] J. H. Huckans, J. R. Williams, E. L. Hazlett, R. W. Stites, and K. M. O'Hara, *Phys. Rev. Lett.* **102**, 165302 (2009), URL <http://link.aps.org/doi/10.1103/PhysRevLett.102.165302>.
- [19] S. Nakajima, M. Horikoshi, T. Mukaiyama, P. Naidon, and M. Ueda, *Phys. Rev. Lett.* **105**, 023201 (2010), URL <http://link.aps.org/doi/10.1103/PhysRevLett.105.023201>.
- [20] G. Barontini, C. Weber, F. Rabatti, J. Catani, G. Thalhammer, M. Inguscio, and F. Minardi, *Phys. Rev. Lett.* **103**, 043201 (2009), URL <http://link.aps.org/doi/10.1103/PhysRevLett.103.043201>.
- [21] R. S. Bloom, M.-G. Hu, T. D. Cumby, and D. S. Jin, *Phys. Rev. Lett.* **111**, 105301 (2013), URL <http://link.aps.org/doi/10.1103/PhysRevLett.111.105301>.
- [22] R. Pires, J. Ulmanis, S. Häfner, M. Repp, A. Arias, E. D. Kuhnle, and M. Weidemüller, *Phys. Rev. Lett.* **112**, 250404 (2014), URL <http://link.aps.org/doi/10.1103/PhysRevLett.112.250404>.
- [23] S.-K. Tung, K. Jiménez-García, J. Johansen, C. V. Parker, and C. Chin, *Phys. Rev. Lett.* **113**, 240402 (2014), URL <http://link.aps.org/doi/10.1103/PhysRevLett.113.240402>.
- [24] B. Huang, L. A. Sidorenkov, R. Grimm, and J. M. Hutson, *Phys. Rev. Lett.* **112**, 190401 (2014), URL <http://link.aps.org/doi/10.1103/PhysRevLett.112.190401>.
- [25] T. Lompe, T. B. Ottenstein, F. Serwane, K. Viering, A. N. Wenz, G. Zürn, and S. Jochim, *Phys. Rev. Lett.* **105**, 103201 (2010), URL <http://link.aps.org/doi/10.1103/PhysRevLett.105.103201>.
- [26] S. Knoop, F. Ferlaino, M. Mark, M. Berninger, H. Schöbel, H.-C. Nägerl, and R. Grimm, *Nature Physics* **5**, 227 (2009).
- [27] M. Zaccanti, B. Deissler, C. D'Errico, M. Fattori, M. Jonas-Lasinio, S. Müller, G. Roati, M. Inguscio, and G. Modugno, *Nature Physics* **5**, 586 (2009).
- [28] N. Gross, Z. Shotan, S. Kokkelmans, and L. Khaykovich, *Phys. Rev. Lett.* **103**, 163202 (2009), URL <http://link.aps.org/doi/10.1103/PhysRevLett.103.163202>.
- [29] A. Zenesini, B. Huang, M. Berninger, H.-C. Nägerl, F. Ferlaino, and R. Grimm, *Phys. Rev. A* **90**, 022704 (2014), URL <http://link.aps.org/doi/10.1103/PhysRevA.90.022704>.
- [30] M.-G. Hu, R. S. Bloom, D. S. Jin, and J. M. Goldwin, *Phys. Rev. A* **90**, 013619 (2014), URL <http://link.aps.org/doi/10.1103/PhysRevA.90.013619>.
- [31] P. Dyke, S. E. Pollack, and R. G. Hulet, *Phys. Rev. A* **88**, 023625 (2013), URL <http://link.aps.org/doi/10.1103/PhysRevA.88.023625>.
- [32] Y. Wang and B. D. Esry, *New J. Phys.* **13**, 035025 (2011), URL <http://stacks.iop.org/1367-2630/13/i=3/a=035025>.
- [33] Y. Wang, J. P. D'Incao, H.-C. Nägerl, and B. D. Esry, *Phys. Rev. Lett.* **104**, 113201 (2010), URL <http://link.aps.org/doi/10.1103/PhysRevLett.104.113201>.
- [34] U. Eismann, L. Khaykovich, S. Laurent, I. Ferrier-Barbut, B. S. Rem, A. T. Grier, M. Delehayé, F. Chevy, C. Salomon, L.-C. Ha, et al., *Phys. Rev. X* **6**, 021025 (2016), URL <http://link.aps.org/doi/10.1103/PhysRevX.6.021025>.
- [35] B. S. Rem, A. T. Grier, I. Ferrier-Barbut, U. Eismann, T. Langen, N. Navon, L. Khaykovich, F. Werner, D. S. Petrov, F. Chevy, et al., *Phys. Rev. Lett.* **110**, 163202 (2013), URL <http://link.aps.org/doi/10.1103/PhysRevLett.110.163202>.
- [36] P. K. Sørensen, D. V. Fedorov, A. S. Jensen, and N. T. Zinner, *Phys. Rev. A* **88**, 042518 (2013), URL <http://link.aps.org/doi/10.1103/PhysRevA.88.042518>.
- [37] B. Huang, L. A. Sidorenkov, and R. Grimm, *Phys. Rev. A* **91**, 063622 (2015), URL <http://link.aps.org/doi/10.1103/PhysRevA.91.063622>.



- 1103/PhysRevA.91.063622.
- [38] Y. Wang, J. P. D’Incao, and B. D. Esry (Academic Press, 2013), vol. 62 of *Adv. At. Mol. Opt. Phys.*, chap. 1, pp. 1 – 115, URL <http://www.sciencedirect.com/science/article/pii/B9780124080904000013>.
- [39] J. R. Taylor, *Scattering Theory* (Dover Publications, 2012), ISBN 9780486142074.
- [40] I. Simbotin and R. Côté, *Chem. Phys.* **462**, 79 (2015), ISSN 0301-0104, URL <http://www.sciencedirect.com/science/article/pii/S0301010415001834>.
- [41] J. P. D’Incao and B. D. Esry, *Phys. Rev. Lett.* **94**, 213201 (2005), URL <http://link.aps.org/doi/10.1103/PhysRevLett.94.213201>.
- [42] F. W. J. Olver and L. C. Maximon, *NIST Handbook of Mathematical Functions* (Cambridge University Press, 2010), chap. 10, ISBN 9780521192255, URL <https://books.google.com/books?id=3I15Ph1Qf38C>.